Large Uniform Copper 1,3,5-Benzenetricarboxylate Metal-Organic-Framework Particles from Slurry Crystallization and Their Outstanding CO_2 Gas Adsorption Capacity

Chunfeng Xue,[a] Enyang Wang,[a] Lin Feng,[a] Qingchun Yuan,[b] Xiaogang Hao[a] and Bo Xiao*[c]*

[a] College of Chemistry and Chemical Engineering, Taiyuan University of Technology, Taiyuan, 030024, P. R. China, E-mail: cfxue@fudan.edu.cn
[b] Engineering and Applied Science, Aston University, Birmingham B4 7ET, UK
[c] School of Chemistry and Chemical Engineering, Queen's University Belfast, Belfast BT9 5AG, UK, E-mail: b.xiao@qub.ac.uk

KEYWORDS: carbon dioxide adsorption, slurry crystallization, metal organic framework, synthesis, cost-effective

ABSTRACT: To prepare more and better metal organic frameworks (MOFs) from less solvent for capturing greenhouse gas, a modified slurry crystallization (MSC) method has been first demonstrated for making MOF copper 1, 3, 5-benzenetricarboxylate from a solvent-deficient system. One outstanding advantage is its drastic reduction of solvent consumption and waste liquid in the whole synthesis. In a typical process, the mass ratio of ethanol to the solid reactants is ~ 0.52, which is only about 0.35% ~ 7.5% of that used in conventional processes. A high yield of ~ 98.0 % is easily achieved for the product with uniform size up to 160 μm. The obtained MOFs demonstrate the characteristic microporous network with a surface area of ~1851 $m^2\ g^{-1}$ and a pore volume of ~0.78 $cm^3\ g^{-1}$, which benefit to adsorb high quantity of CO_2 ~ 6.73 mol kg^{-1} at ordinary pressure. X-ray diffraction studies indicate that the MOFs possess an outstanding diffraction intensity ratio of the crystal plane (2, 2, 2) to (2, 0, 0), $I_{(222)}/I_{(200)}$ = 22.4. The MSC method provides a cost-effective approach for large-scale production of MOFs with more attractive properties than others. Most importantly, it can significantly cut down the waste liquid and production cost.

1. Introduction

Metal-organic frameworks (MOFs) standing out from microporous materials are mainly due to their unique characteristics, such as high surface area, structural tunability and diverse functionality. Judicious assembly of metal cations and organic ligands as building blocks allows bespoke MOFs' structure to be constructed to best suit the requirements for various applications, e.g. hydrogen storage, gas separation, CO_2 capture and catalyst supporter.[1-4] There are many key factors influencing their industrial implementation,[2] one of which is their cost dominated by ligands and solvents. In addition to the ligands, a large amount of organic solvent used for mixing the initial reactants and facilitating the MOF crystallization.[5, 6] Although the solvent plays the key roles in the crystallization process, i.e. regulating the formation of the different coordination environment; acting as structure directing agent to control the configuration of the structure and as a guest molecule to stabilize MOF structure, the mechanism of the solvent mediating specific MOF crystallization in fact still remains unclear. This inevitably results in the irrational consumption of solvents, high running cost and serious environmental concerns.

Among the diverse MOFs, a typical MOF coded as HKUST-1 (also as $Cu_3(BTC)_2(H_2O)_3 \cdot xH_2O$) has been widely studied.[7] Compared with most of other MOFs, its starting materials are relatively cheaper. Particularly, the bezenetricarboxylic (BTC) acid only costs about \$ 20.0 kg^{-1} or less.[8] A wide range of copper sources including $Cu(NO_3)_2$, $Cu(CH_3COO)_2$, $Cu(OH)_2$ and even metal Cu (by Galvanic corrosion) are available for making HKUST-1 in different solvents.[9] HKUST-1 with different specific surface area can be synthesized in different yields by solvo/hydrothermal method at 348-

393 K.[10-13] For example, refluxing dimethylformamide (DMF) at 423 K produces HKSUT-1 in a 65% yield. Subsequently, high surface area can be achieved by a thorough solvent displacing operation.[14] Other approaches including microwave-assisted synthesis,[15] electrochemical route,[4] and ultrasonic synthesis,[16] were also investigated.[17] It should be noted that a large amount of organic solvent, methanol (MeOH),[4] ethanol (EtOH),[7] DMF,[14] or dimethyl sulfoxide (DMSO),[18] are used in the above processes accompanying with plenty of waste liquid.[19] Their mass ratios of organic solvent to solid reactants in preparation process are calculated at about 7 ~ 150. Most of the MOF crystals are centered at around 1.0 μm in diameter. Alternatively, solventless mechano-chemical synthesis has been developed for preparing HKUST-1. However, a large amount of EtOH is still required to purify and activate the products.[17, 20-23] The mechanical impact process also encounter the risk of serious explosion. From a commercial and sustainable viewpoint, using cheap and recyclable solvent and maximally reducing waste liquid to save processing energy should be taken into consideration. Water is a perfect green solvent. However, when water is exclusively used in the synthesis system, the one-dimensional zigzag chain structure $Cu(BTC)(H_2O)_3$ (catena-triaqua-μ-(1,3,5-benzenetricarboxylate)-copper(II)) is formed only.[5] Feasibly, a rationally small amount of organic solvent is required for the formation of the ideal HKUST-1 structure. Based on this, a cost-effective strategy to produce a high quality MOF using less solvent is desired.

Recently, slurry or suspension crystallization technique has been studied for co-crystallization of pharmaceuticals, aiming to modify drug property.[24] We think this approach can be used for making MOFs and rationally reduce the consumption of solvent. Meanwhile, a high spacetime yield can be expected. In this work, taken the MOF HKUST-1 as a model, a modified slurry

crystallization (MSC) is demonstrated to synthesize it in a cost-effective style. The evolution of its morphology and property dependent on the method has been mainly investigated.

2. Experimental

2.1 Chemicals: 1, 3, 5-benzene tricarboxylic acid (H_3BTC, >99%) was used as obtained from Maya Reagent Company. Copper(II) nitrate trihydrate ($Cu(NO_3)_2 \cdot 3H_2O$, >99%), ethanol (EtOH, >99.7%) were purchased from Tianjin Kemiou Chemical Reagent Co. All raw materials were used without further purification.

2.2 Preparation of HKUST-1 using modified slurry crystallization (MSC) method: The stoichiometric molar ratio of $Cu(NO_3)_2 \cdot 3H_2O$ to H_3BTC is kept at 3:2 for all the experiments, also the volumetric ratio of EtOH/H_2O at 1:1 (**Table 1**). The relative quantity of solvent to the solid reactants is varied from 0.13 to 2.07, allowing the effect of solvent amount on the product to be examined. H-1, H-0.5 and H-0.25 use a little amount of EtOH varying from 1.5 to 0.375 mL. Briefly, $Cu(NO_3)_2 \cdot 3H_2O$ (1.44 g, 6.0 mmol) is dissolved in the pre-mixed solution with deionized H_2O (1.5 mL, 1.49 g, 83.09 mmol) and EtOH (1.5 mL, 1.18 g, 25.68 mmol) and stirred at room temperature for 30 min. Then H_3BTC powder (0.84 g, 4.0 mmol) is added in the previous blue solution with further stirring for 60 min. The mass ratio of EtOH to the solid reactants ($Cu(NO_3)_2 \cdot 3H_2O$ plus H_3BTC) (E/S) is calculated at about 0.52. Finally the obtained slurry is sealed in 25 mL autoclave and heated at 383 K for 10 h. After the autoclave is cooled to room temperature, liquid droplets on the upper of autoclave inside are collected and removed. The blue crystal is directly dried at room temperature overnight as as-made sample H-1 without any washing. The space-time yield is calculated at 790.8 kg m^{-3} d^{-1}. In case of preparation of H-2 and H-4, obvious mother liquor is remained at the autoclave bottom and decanted for collecting samples. They are harvested in a yield of around 98%.

2.3 Characterizations: X-ray diffraction (XRD) patterns are recorded on a Rigaku D/Max-3B type X-ray diffractometer with the Cu Kα radiation, (λ= 0.15406 nm, 40 kV, 40 mA) in a scan range of 5-50°. N_2 adsorption-desorption isotherms are measured on JW-BK122 W at 196 °C. Pore size distributions are calculated from Horvath-Kawazoe method. The sample is outgassed at 150 °C for 10 h before measurements. Thermogravimetry (TG) curves of samples are collected on a Netzsch STA 449 F5 TG/DTG instrument. About 5 mg of samples are placed onto an alumina crucible and heated at a ramp of 10 °C·min^{-1} in the range of from 25 to 800 °C in N_2 flow (100 mL·min^{-1}) to analyze thermal stability. SEM images are collected on Field Emission Scanning Electron Microscope JSM-7100F operated at 10 kV. All the samples are coated a thin gold film. The optical light microscopy images are observed with a Leica MS5 binocular eyepiece with transmitted light and polarization filter. The images of isolated crystals are taken with a Nikon COOLPIX 4500 digital camera through a special ocular connection.

2.4 CO_2 adsorption investigation: The CO_2 adsorption isotherms are measured on JW-BK122W. The CO_2 gas with high purity (99.999%) is regulated in a range of 0 – 1.0 bar. First, 0.1 – 0.2 g sample was put into the sample tube and outgassed at 423 K overnight before the testing, then started to measure at room temperature of 295 K. The weight of samples was recorded after the measurement.

3. Results and Discussion

In the MSC process, a thick gel-like mixture of HKUST-1 precursor is initially formed, followed by its crystallization at 383 K for 10 h. Condensed acidic liquid droplets (HNO_3, EtOH and H_2O) aggregate on the upper section inside the autoclave. Semidry crystals in deep turquoise are formed at the bottom of the autoclave. They are collected in an almost calculated yield and

dried in the air without further washing treatment. XRD patterns of the samples are stacked in **Figure 1**. Their peak positions are consistent with the reported HKUST-1 except that detectable impurity appears in the sample H-0.25.[10] However, the ratios of diffraction intensity $I_{(222)}/I_{(200)}$ (2θ = 11.6, 9.5°) with respect to the crystal planes (222) and (200) are obviously varied along with the used solvent quantity (**Table 1)**. In details, the sample H-1 prepared with the E/S ratio of 0.52 exhibits the strongest diffraction intensity (**Figure 1A**), implying the highest crystallinity of this sample compared to the other ones. The enhanced dominant peak at 2θ = 11.6° is observed for all the samples. The largest ratio of $I_{(222)}/I_{(200)}$ is up to 22.438 for the sample H-1. Similar results have been observed for the oriented growth of HKUST-1 either on the $–CH_3$ and –OH functionalized self-assembled monolayer[10] or in a harsh environment.[18] By means of atomic force microscopy and in-situ diffraction analysis,[25-27] it clarifies that the crystal growth prefers to take along [111] orientation. The growth feature well coincides with the extreme supersaturation of the initial mixture and the crystallization conditions.[28] Under the synthesis condition here, the simulation of isothermal vapor-liquid equilibrium has shown that much less molar number of H_2O and EtOH, 6.89 mmol, are in liquid phase at 383 K in a volume of 25 mL with a molar fraction of EtOH 0.03 only, compared with a value of 102.1 mmol in vapor phase equivalent to ~2.5 mL at room temperature, where the molar fraction of EtOH is 0.25. Obviously, in this case, much less amount of liquid presents for the growth of HKUST-1 crystal, which may finally influence MOF particle size. With doubling the E/S ratio (1.03) in the sample H-2, the ratio of $I_{(222)}/I_{(200)}$ decreases to 8.072; and further decreases to 3.225 for the sample H-4 with an E/S values of 2.07 (**Figure 1B, C** and **Table 1)**, which is close to common HKUST-1 from hydrothermal method. From these results, we consider that it is possible to optimize the use of a solvent to control the growth and even the yield of HKUST-1 crystal. For the samples H-0.5

and H-0.25**,** the used solvents are not enough to provide a suitable environment for the crystallization. In details, the solvent is not enough to mix reactants homogeneously and to provide a proper mobility for the undissolved reactants, leading to the formation of the impurity and the incomplete reaction (**Figure 1E, F)**.[5] When the EtOH is only used as the solvent without any added H_2O and the E/S ratio is still kept at 0.52, the obtained sample H-10 shows a very low crystallinity but no detectable impurity from XRD pattern (**Figure 1D)**. Its $I_{(222)}/I_{(200)}$ ratio is similar to that of H-4 (**Table 1**). This result implies that H_2O plays a crucial role in the growth of large HKUST-1 crystals. Similar results have been observed for the HKUST-1 prepared from $Cu(OH)_2$.[9]

Figure 2 shows SEM images of as-made samples H-4, H-2, H-1, H-10, H-0.5, and H-0.25. The sample H-4 (E/S = 2.07) is mainly composed of 13 μm uniform particles and small number of ones in 25-35 μm (**Figure 2A, B**). They are regular and smooth. Just as observed and calculated from its optical photograph (**Figure 3a**, **b**), about 62% particles center at 15 μm in size (**Figure 3c**). In the whole batch sample, it can be seen that a thick layer of small uniform particles gather at the bottom and only a thin layer of large ones stands on the top (**Figure S2a**). When the ratio E/S reduces to 1.03, the sample H-2 particles tend to become bigger. It is mainly composed of 20-60 μm and 100-140 μm regular crystals, (**Figure 2C, D**). Their surfaces become rough compared to the sample H-4. Its particle size distribution (**Figure 3f)** is also calculated at about 41.3% and 43.5% separately according to its optical images (**Figure 3d, e**). With the ratio E/S further decreasing to 0.52, the sample H-1 exhibits uniform large octahedral crystals (**Figure 2E, F**). About 92 % of the crystals increase to 80-160 μm in size (**Figure 3g, h, i**). What's more, their color turns thick because of the enhanced size, which can be observed from its

overall photograph (**Figure S2c**). All the results indicate that minute solvent benefits to get deep turquoise and large particle (**Figure S2c**). Combining with previous XRD results, they suggest a preferentially oriented growth of crystals in such a solvent-deficient system. Similar crystal oriented growth and morphology evolution was observed by increasing the concentration of KNO_3 in EtOH/H_2O solution.[29] Small size particles mainly contain the high-energy {100} facets, whereas the larger crystals have the developed low-energy {111} facets. To some extent, this might be similar to the reduction of the ratio E/S, i.e. increasing the concentration of Cu^{2+} and BTC. Adjusting the solution concentration will impact the interaction between Cu^{2+} and BTC and promote their assembling along one direction towards the low-energy facets. Similarly, small changes of crystal size and morphology dependent on the concentration also happened in microwave and hydrothermal synthesis of HKUST-1.[15,30] In the absence of H_2O, the small but uniform crystals (2-14 μm) are observed in the sample H-10 (**Figure 2G, H and Figure 3j, k, l**), indicating the importance of H_2O in mediating crystals size. Interestingly, the very tiny particles take on bluish green color different from others (**Figure S3d**). For the sample H-0.5 prepared from E/S = 0.26, particles are aggregating into irregular shapes in around 100 μm (**Figure 2I, J**). They are HKUST-1 crystals but with low crystallinity. It can be seen that they are covered with some amorphous species (**Figure 2J**). From its optical image (**Figure S1b and Figure S2e)**, it can be also observed that tiny white particles are mixed with HKUST-1 crystals. Combining the above results, we can deduce that the white particle as impurity is part of unreacted ligand. Particularly, in the case of the sample H-0.25 derived from the further reduced ratio E/S = 0.13, the sample displays irregular shape with different size (**Figure 2K, L**). Many white particles appear in the

product (**Figure S1b, c and Figure S2f**), implying the existence of impurity composed of unreacted ligand and unknown phase concluded from the XRD result.[31] Their FTIR spectra also exhibit some difference between them (**Figure 4**). Two obvious bands ascribing to the stretching vibrations of C=O (1709 cm^{-1}) and C-O (1232 cm^{-1}) labeled by dashed lines are observed for samples H-0.5 and H-0.25 (**Figure 4e, f**), which are the characteristic bands of ligand H_3BTC. Therefore, their presence in FTIR spectra indicates the unreacted ligand staying in the samples. The results coincide with the observations from photographical images above. Noticeably, the two vibration bands are drastically weakened even disappeared in the other HKUST-1 samples including H-1, H-2, H-4 and H-10 (**Figure 4a-d**), implying no ligand remaining in them. That means the obtained sample is highly pure and agrees with the conclusions from their XRD patterns and images.

Although crystal size and morphology of samples depend on the preparation conditions, their thermal stability that is determined by the framework structure is not affected. This is reflected in the TG profiles in **Figure 5**. MOFs H-1, H-2 and H-4 show weight loss ~20.4 wt% at about 100 ºC that can be ascribed to the removal of physically adsorbed EtOH and H_2O (**Figure 5a-c**). A further weight loss 4.6 wt% occurring at ~150 ºC is related to the removal of the coordinated H_2O (**Figure 5a-c**). When the temperature rises to ~ 355 ºC, the frameworks become thermally unstable (**Figure 5a-c**).[7, 32] H-0.5 performs differently, because it is a mixture of HKUST-1 crystals and the unreacted ligand (**Figure 5e**). The results are consistent with the conclusion from above FT-IR results and images. H-10 was obtained from anhydrous EtOH. At ~100 ºC, its weight loss is only 14.9 wt% (**Figure 5d**) contributed from the removal of adsorbed ethanol, which is

different from and less than that of other MOFs crystallized in ethanol-water solution. As a result, the sample H-10 reasonably shows the least total weight loss among all the as-made samples. If we suppose that both sample H-10 and H-1 have the same pore volume, the ratio of weight loss below 100 ºC is calculated at 0.73 and very close to the density ratio 0.79 of EtOH to H_2O. Considering the relative polarity of ethanol to water, 0.654, this infers that the HKUST-1 has affinity to adsorb more polar water molecules.

N_2 adsorption isotherms of samples H-1, H-2, H-4 and H-10 are of type I curves corresponding to microporous materials but exhibit different adsorption volumes (**Figure 6** (**A**)**a-d**). All the samples display fairly narrow pore size distributions centered at about 0.62 nm **(Figure 6** (**B**)**a-d**), coinciding with their micropore structure. Amazingly, the sample H-1 achieves a high BET surface area up to 1851 $m^2\ g^{-1}$ and pore volume of 0.78 $cm^3\ g^{-1}$ (**Figure 6** (**A**)**a**), which is in the scope of high surface area materials (**Table 2)**. For samples H-2 and H-4, their surface areas are 1539 and 1258 $m^2\ g^{-1}$, pore volumes 0.63 and 0.48 $cm^3\ g^{-1}$, respectively. In case of sample H-10 with rather small size, it displays the smallest surface area (932 $m^2\ g^{-1}$) and pore volume (0.43 $cm^3\ g^{-1}$) among them. According to the above XRD results (**Figure 1a-d**), no detectable peak at 2θ = 36.4º can be observed for possible impurity Cu_2O present in the products. Therefore, the difference between their surface areas is directly in relation to their particle sizes. Predictably, the large H-1 particles will perform better gas adsorption than others.

Figure 7 shows the results of CO_2 gas adsorption over the samples H-1, H-2, and H-4. The highest adsorption capacity of 6.73 mol kg^{-1} (**Figure 7a)**, has been achieved by the sample H-1 composed of the biggest and most uniform crystals among all the samples (**Figure 2E, F**). As far as we know, this capacity is higher than the published results at the

same adsorption conditions.[33] Samples H-2 and H-4 with small particle size adsorb CO_2 of 5.06 and 3.92 mol kg^{-1} (**Figure 7b, c)**, respectively. The results clearly line out the effect of particle size on CO_2 gas adsorption capacity of samples HKUST-1. Compared with the previously reported CO_2 adsorption capacity of 1.0 – 4.5 mol kg^{-1} over small size HKUST-1,[34-39] we tentatively believe that the particle H-1 with large size can provide longer porous channels and hence accommodate more CO_2 molecules than others.

Basing on the above observation, we propose the difference between the solvo/hydrothermal method and the MSC adopted in this study as shown in **Figure 8**. Usually, MOFs are solvo/hydrothermally prepared in systems involving a large amount of solvents (**Figure 8a**), which mainly follow solution-mediated transport mechanism for crystal growth. The mechanism generally involves the complete dissolution of precursors and necessary mobility of the dissolved species by solution-mediated transport to nucleate for crystal formation.[40] Herein, $Cu(NO_3)_2 \cdot 3H_2O$ and H_3BTC can be easily dissolved in a huge amount of solvent. A gas-liquid phase equilibrium is established between the mixed vapor (H_2O, EtOH and HNO_3) and the mother liquor during the crystallization process. In the whole preparation process, the liquor always stays and establishes a dynamic equilibrium between dissolution and crystallization of HKUST-1 crystals. The liquor containing part of reactants is finally drained away as waste liquid. As a result, this leads to a low yield and environmental pollution. The polydispersity in the conventional synthesis has been explained by simultaneous nucleation and growth.[41]

In the MSC process (**Figure 8b**), the reaction slurry is supersaturated by significantly reducing solvent amount, which is about 10% or less than that of hydrothermal method. Undoubtedly, the usage of small quantity solvent diminishes the formation of large

amount of mother liquor from the first place. Moreover, most of the mother liquor during the crystallization process presents as the vapor phase in the upper section of the reactor, which is apparently separated from the formed crystals at the bottom of reactor. Thus, the absence of liquid phase containing high concentration of MOF crystals can not facilities new nucleation favourably.[42,43] Once nucleation completes during the slurry making, crystals will equally grow from the existing nuclei made from the building blocks, which allow the uniform crystals to be formed along a low energy favor orientation. For example, the sample H-1 has fairly uniform size distribution (**Figure 2i**) than the sample H-2 and H-4, its particle is also much bigger than that of conventional synthesis. Finally, the large size of the uniform particles may lead to a high diffraction ratio of crystal plane (222) to (200) (**Figure** 1a). Here, such a MSC process is similar to the confined evaporation of a clear precursor solution for patterning HKUST-1.[18] Since no obvious liquor is left, the large product particles can be easily harvested in an almost calculated yield.

4. Conclusions

In summary, we have demonstrated the MSC method for the first time for the complete conversion of a solvent-deficient slurry into a pure MOF material. This method can produce MOF HKUST-1 with uniform size up to 160 μm with less solvent in a high yield. The large HKUST-1 particles exhibit high surface area of 1851 m^2 g^{-1} and an excellent CO_2 adsorption capacity of 6.73 mol kg^{-1} at normal pressure. The MSC method is of significant interest for producing MOFs in a cost-effective manner and avoiding to handle large amount of solvent and waste liquid. Most importantly, the MOF derived from the

MSC method displays more attractive property and application performance than others. Its feasibility for synthesizing other types of MOFs is being under investigation.

Acknowledgments

The authors acknowledge the financial supports from China Scholarship Council (No. 201506935028), Key Scientific and Technological Projects of Shanxi Province (No. MD2014-09), and Youth Foundation of Taiyuan University of Technology (No. 2015MS015).

References

1 Cui, X.; Chen, K.; Xing, H.; Yang, Q.; Krishna, R.; Bao, Z.; Wu, H.; Zhou, W.; Dong, X.; Han, Y.; Li, B.; Ren, Q.; Zaworotko, M. J.; Chen, B.; Pore chemistry and size control in hybrid porous materials for acetylene capture from ethylene. *Science*, **2016**, *353*(6295), 141-144.

2 Czaja, A. U.; Trukhan, N.; Muller, U.; Industrial applications of metal–organic frameworks. *Chem. Soc. Rev.*, **2009**, *38*(5), 1284-1293.

3 Zacher, D.; Shekhah, O., Woll, C.; Fischer, R. A.; Thin films of metal-organic frameworks. *Chem. Soc. Rev.*, **2009**, *38*(5), 1418-1429.

4 Mueller, U.; Schubert, M.; Teich, F., Puetter, H.; Schierle-Arndt, K.; Pastre, J.; Metal-organic frameworks-prospective industrial applications. *J. Mater. Chem.*, **2006**, *16*(7), 626-636.

5 Gascon, J.; Aguado S.; Kapteijn, F.; Manufacture of dense coatings of $Cu_3(BTC)_2$ (HKUST-1) on α-alumina. *Micropor. Mesopor. Mat.*, **2008**, *113*(1), 132-138.

6 Zhang, B.; Zhang, J.; Liu, C.; Sang, X.; Peng, L.; Ma, X.; Wu, T.; Han, B.; Yang, G.; Solvent determines the formation and properties of metal-organic frameworks. *RSC Adv.*, **2015**, *5*, 37691-37696.

7 Chui, S. S. Y.; Lo, S. M. F.; Charmant, J. P. H.; Orpen, A. G.; Williams, I. D.; A chemically functionalizable nanoporous material $[Cu_3(TMA)_2(H_2O)_3]_n$. *Science*, **1999**, *283*(5405), 1148-1150.

8 Liu, J.; Thallapally, P. K.; McGrail, B. P.; Brown, D. R.; Liu, J.; Progress in adsorption-based CO_2 capture by metal–organic frameworks. *Chem. Soc. Rev.* **2012**, *41*, 2308-2322.

9 Majano, G.; Pérez-Ramírez, J.; Scalable room-temperature conversion of copper(II) hydroxide into HKUST-1 ($Cu_3(btc)_2$). *Adv. Mater.*, **2013**, *25*(7), 1052-1057.

10 Biemmi, E.; Scherb, C.; Bein, T.; Oriented growth of the metal organic framework $Cu_3(BTC)_2(H_2O)_3 \cdot xH_2O$ tunable with functionalized self-assembled monolayers, *J. Am. Chem. Soc.*, **2007**, *129*(26), 8054-8055.

11 Roswell, J. L. C.; Yaghi, O. M.; Effects of functionalization, catenation, and variation of the metal oxide and organic linking units on the low-pressure hydrogen adsorption properties of metal−organic frameworks. *J. Am. Chem. Soc.*, **2006**, *128*(4), 1304-1315.

12 Alaerts, L.; Séguin, E.; Poelman, H.; Thibault-Starzyk, F.; Jacobs, P. A.; De Vos, D. E.; Probing the lewis acidity and catalytic activity of the metal–organic framework [Cu3(btc)2] (BTC=Benzene-1,3,5-tricarb-oxylate), *Chem. Eur. J.*, **2006**, *12*(28), 7353-7363.

13 Zacher, D.; Baunemann, A.; Hermes S.; Fischer, R. A.; Deposition of microcrystalline $[Cu_3(btc)_2]$ and $[Zn_2(bdc)_2(dabco)]$ at alumina and silica surfaces modified with patterned

self assembled organic monolayers: evidence of surface selective and oriented growth. *J. Mater. Chem.*, **2007**, *17*(27), 2785-2792.

14 Krawiec, P.; Kramer, M.; Sabo, M.; Kunschke, R.; Fröde, H.; Kaskel, S.; Improved hydrogen storage in the metal-organic framework $Cu_3(BTC)_2$. *Adv. Eng. Mater.* **2006**, *8*(4), 293-296.

15 Y. K. Seo, G. Hundal, I. T. Jang, Y. K. Hwang, C. H. Jun and J. S. Chang, Microwave synthesis of hybrid inorganic–organic materials including porous $Cu_3(BTC)_2$ from Cu(II)-trimesate mixture, *Micropor. Mesopor. Mat.*, **2009**, *119*(1), 331-337.

16 Li, Z.; Qiu, L.; Xu, T.; Wu, Y.; Wang, W.; Wu Z.; Jiang, X.; Ultrasonic synthesis of the microporous metal–organic framework $Cu_3(BTC)_2$ at ambient temperature and pressure: An efficient and environmentally friendly method. *Mater. Lett.*, **2009**, *63*(1), 78-80.

17 Schlesinger, M.; Schulze, S.; Hietschold, M.; Mehring, M.; Evaluation of synthetic methods for microporous metal–organic frameworks exemplified by the competitive formation of $[Cu_2(btc)_3(H_2O)_3]$ and $[Cu_2(btc)(OH)(H_2O)]$, *Micropor. Mesopor. Mater.* **2010**, *132*(1), 121-127.

18 Ameloot, R.; Gobechiya, E.; Uji-i, H.; Martens, J. A.; Hofkens, J.; Alaerts, L.; Sels, B. F.; De Vos, D. E.; Direct patterning of oriented metal–organic framework crystals via control over crystallization kinetics in clear precursor solutions. *Adv. Mater.*, **2010**, *22*(24), 2685-2688.

19 Reinsch, H.; "Green" synthesis of metal-organic frameworks. *Eur. J. Inorg. Chem.* **2016**, *2016*(27), 4290-4299.

20 Yuan, W.; Garay, A. L.; Pichon, A.; Clowes, R.; Wood, C. D.; Cooper, A. I.; James, S. L.; Study of the mechanochemical formation and resulting properties of an archetypal MOF:

$Cu_3(BTC)_2$ (BTC = 1,3,5-benzenetricarboxy-late). *CrystEngComm*, **2010**, *12*(12), 4063-4065.

21 Klimakow, M.; Klobes, P.; Thünemann, A. F.; Rademann, K.; Emmerling, F.; Mechanochemical synthesis of metal−organic frameworks: A fast and facile approach toward quantitative yields and high specific surface areas. *Chem. Mater.*, **2010**, *22*(18), 5216-5221.

22 Majano, G.; Martin, O.; Hammes, M.; Smeets, S.; Baerlocher, C.; Pérez-Ramírez, J.; Solvent-mediated reconstruction of the metal–organic framework HKUST-1 ($Cu_3(BTC)_2$). *Adv. Funct. Mater.* **2014**, *24*(25), 3855-3865

23 Sun, X.; Li, H.; Li, Y.; Xu, F.; Xiao, J.; Xia, Q.; Li, Y.; Li, Z.; A novel mechanochemical method for reconstructing the moisture-degraded HKUST-1. *Chem. Commun.*, 2015, **51**, 10835-10838.

24 Zhang, G. G. Z.; Henry, R. F.; Borchardt, T. B.; Lou, X.; Efficient co-crystal screening using solution-mediated phase transformation. *J. Pharm. Sci.*, **2007**, *96*(5), 990-995.

25 Shoaee, M.; Anderson, M. W.; Attfield, M. P.; Crystal growth of the nanoporous metal–organic framework HKUST-1 revealed by in situ atomic force microscopy. *Angew. Chem. Int. Ed.*, **2008**, *47*(44), 8525-8528.

26 Shoaee, M.; Agger, J. R.; Anderson, M. W.; Attfield, M. P.; Crystal form, defects and growth of the metal organic framework HKUST-1 revealed by atomic force microscopy. *CrystEngComm*, **2008**, *10*(6), 646-648.

27 Millange, F.; Medina, M. I.; Guillou, N.; Férey, G.; Golden, K. M.; Walton, R. I.; Time-resolved in situ diffraction study of the solvothermal crystallization of some prototypical metal–organic frameworks. *Angew. Chem. Int. Ed.*, **2010**, *49*(4), 763-766.

28 R. L. Parker, in *Solid State Physics*, eds. F. S. Henry Ehrenreich and T. David, Academic Press, 1970, Vol. 25, pp. 151-299.

29 Liu, Q.; Yang, J. M.; Jin, L. N.; Sun, W. Y.; Metal ion induced porous HKUST-1 nano/microcrystals with controllable morpho-logy and size, *CrystEngComm*, **2016**, *18*(22), 4127-4132.

30 Biemmi, E.; Christian, S.; Stock, N.; Bein, T.; High-throughput screening of synthesis parameters in the formation of the metal-organic frameworks MOF-5 and HKUST-1. *Micropor. Mesopor. Mater.*, **2009**, *117*(1), 111-117.

31 Paseta, L.; Potier, G.; Sorribas, S.; Coronas, J., Solventless synthesis of MOFs at high pressure. *ACS Sustainable Chem. Eng.,* **2016**, *4* (7), 3780-3785.

32 Wee, L. H.; Lohe, M. R.; Janssens, N.; Kaskel S.; Martens, J. A.; Fine tuning of the metal-organic framework $Cu_3(BTC)_2$ HKUST-1 crystal size in the 100 nm to 5 micron range. *J. Mater. Chem.*, 2012, **22**, 13742-13746.

33 Min Wang, Q.; Shen, D.; Bülow, M.; Ling Lau, M.; Deng, S.; Fitch, F. R.; Lemcoff, N. O.; Semanscin, J.; Metallo-organic molecular sieve for gas separation and purification. *Micropor. Mesopor. Mat.*, **2002**, *55*(2), 217-230.

34 Mao, Y.; Chen, D.; Hu, P.; Guo, Y.; Ying, Y.; Ying, W.; Peng, X.; Hierarchical mesoporous metal–organic frameworks for enhanced CO_2 capture. *Chem. Eur. J.*, **2015**, *21*(43), 15127-15132.

35 Bahamon D.; Vega, L. F.; Systematic evaluation of materials for post-combustion CO_2 capture in a temperature swing adsorption process. *Chem. Eng. J.*, **2016**, *284*, 438-447.

36 Cao, Y.; Zhao, Y.; Song, F.; Zhong, Q.; Alkali metal cation doping of metal-organic framework for enhancing carbon dioxide adsorption capacity. *J Energy Chem.*, **2014**, *23*(4), 468-474.

37 Al-Janabi, N.; Hill, P.; Torrente-Murciano, L.; Garforth, A.; Gorgojo, P.; Siperstein, F.; Fan, X.; Mapping the Cu-BTC metal–organic framework (HKUST-1) stability envelope in the presence of water vapour for CO_2 adsorption from flue gases. *Chem. Eng. J.*, **2015**, *281*, 669-677.

38 Li, J. R.; Ma, Y.; McCarthy, M. C.; Sculley, J.; Yu, J.; Jeong, H. K.; Balbuena, P. B.; Zhou, H. C.; Carbon dioxide capture-related gas adsorption and separation in metal-organic frameworks. *Coordin. Chem. Rev.*, **2011**, *255*(15), 1791-1823.

39 Liang, Z.; Marshall, M.; Chaffee, A. L.; CO_2 adsorption-based separation by metal organic framework (Cu-BTC) versus zeolite (13X). *Energ. Fuel.*, **2009**, *23*(5), 2785-2789.

40 Cundy, C. S.; Cox, P. A.; The hydrothermal synthesis of zeolites: Precursors, intermediates and reaction mechanism, *Micropor. Mesopor. Mat.*, **2005**, *82*(1-2), 1-78.

41 Zacher, D.; Liu, J.; Huber, K.; Fischer, R. A.; Nanocrystals of $[Cu_3(btc)_2]$ (HKUST-1): a combined time-resolved light scattering and scanning electron microscopy study. *Chem. Commun.*, **2009**, 1031-1033.

42 Aizenberg, J.; Black, A. J.; Whitesides, G. M.; Control of crystal nucleation by patterned self-assembled monolayers. *Nature*, **1999**, *398*(6727), 495-498.

43 Briseno, A. L.; Mannsfeld, S. C. B.; Ling, M. M.; Liu, S.; Tseng, R. J.; Reese, C.; Roberts, M. E.; Yang, Y.; Wudl, F.; Bao, Z.; Patterning organic single-crystal transistor arrays. *Nature*, **2006**, *444*(7121), 913-917.

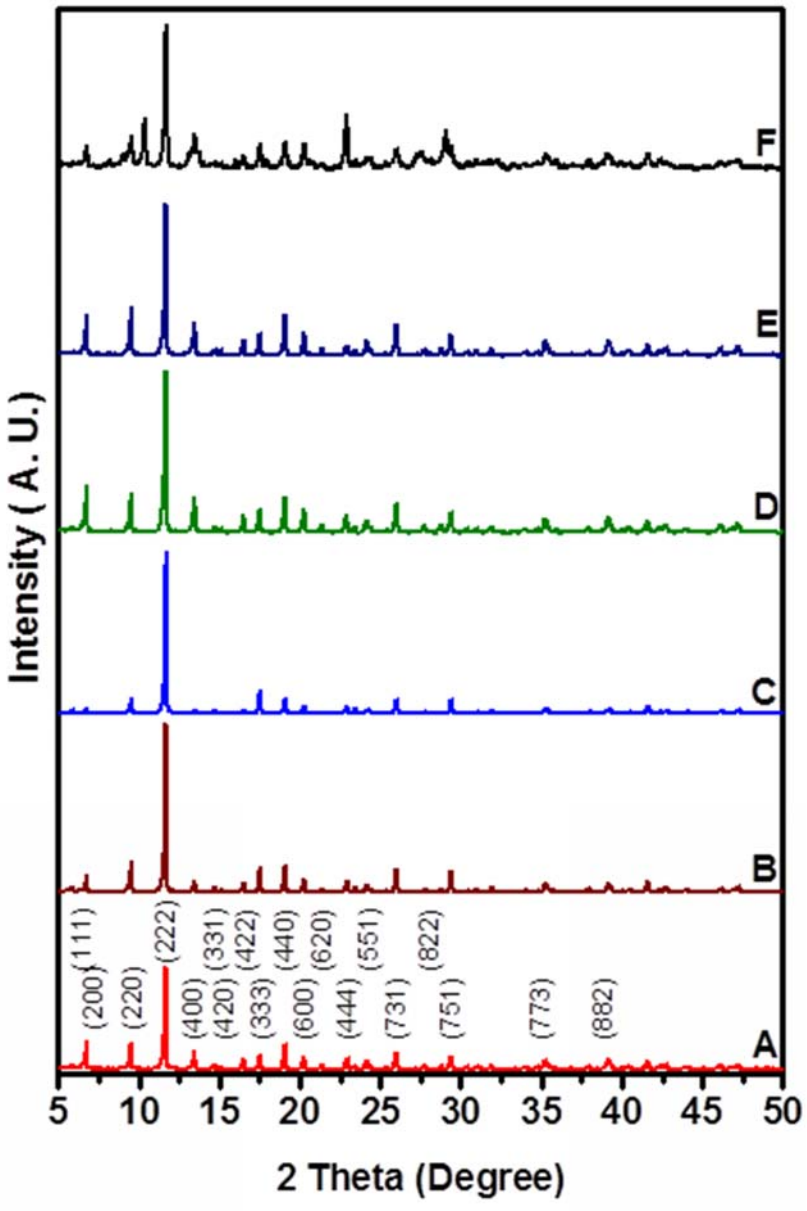

Figure 1. XRD patterns of as-made samples: (A) H-1; (B) H-2; (C) H-4; (D) H-10; (E) H-0.5; and (F) H-0.25 synthesized with different amount of solvent at 383 K for 10 h

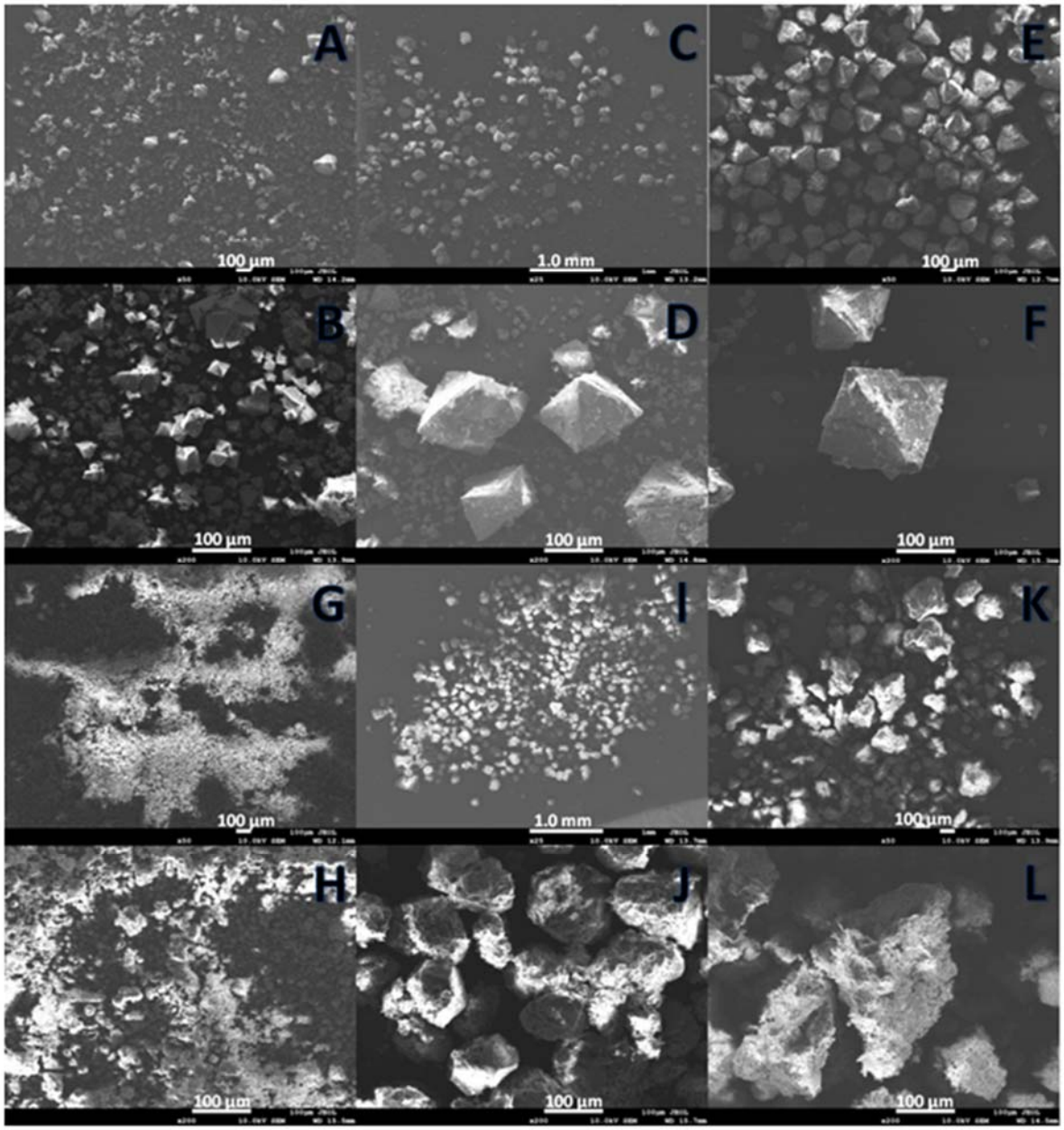

Figure 2. SEM images of as-made samples: (A, B) H-4; (C, D) H-2; (E, F) H-1; (G, H) H-10; (I, J) H-0.5; and (K, L) H-0.25

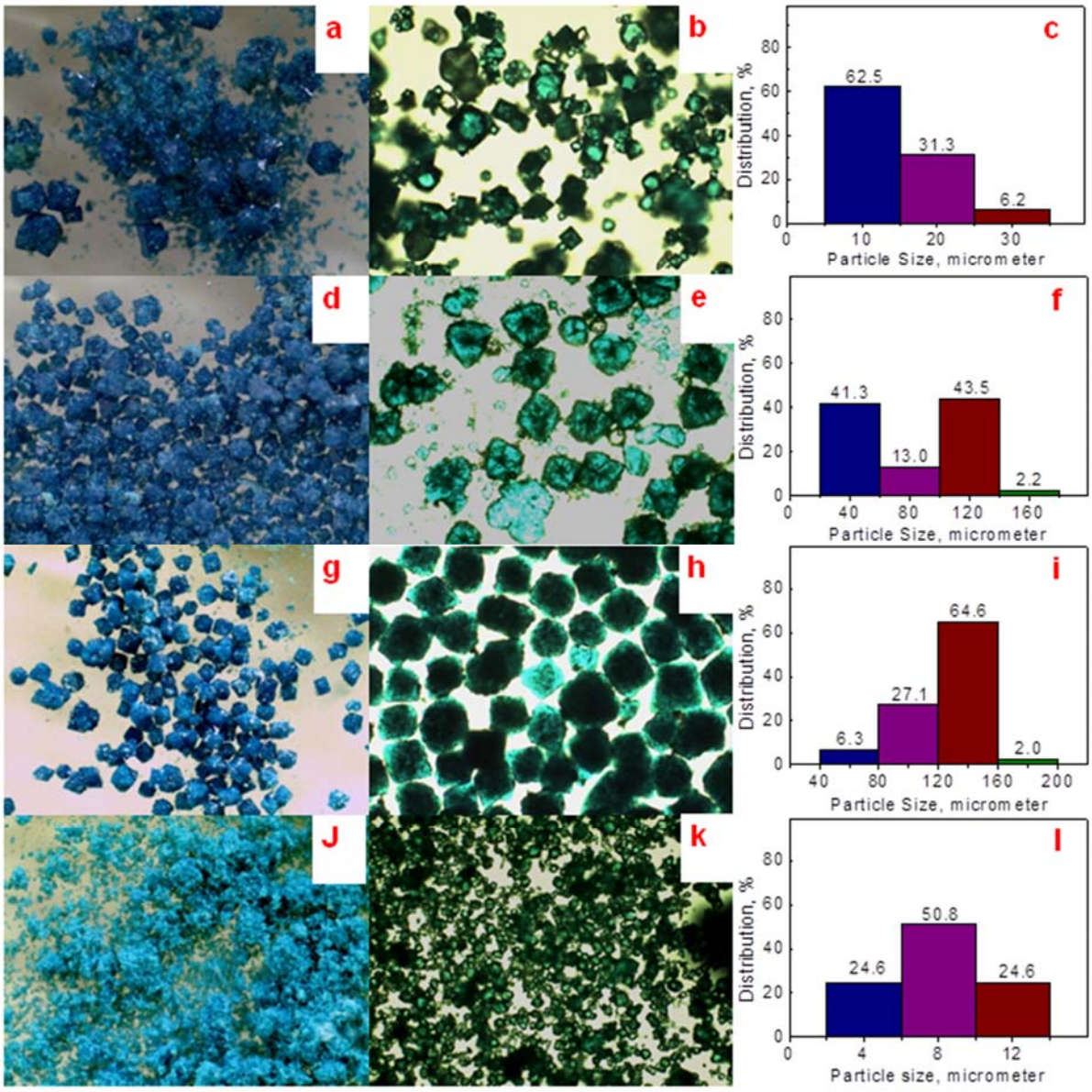

Figure 3. Light microscopy images and particle size distributions of as-made samples: (a, b, c) H-4; (d, e, f) H-2; (g, h, i) H-1; and (j, k, l) H-10

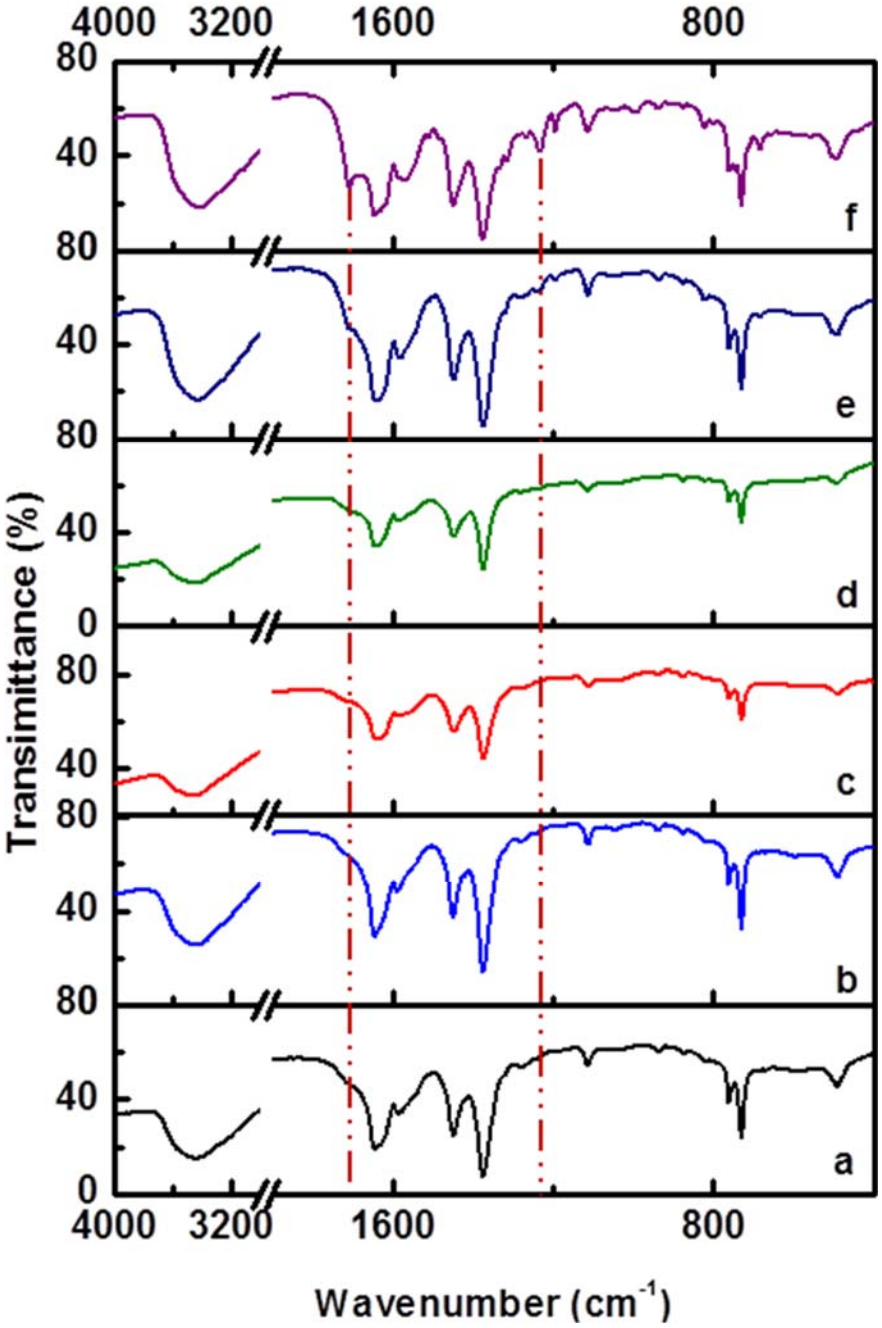

Figure 4. FT-IR spectra of as-made HKUST-1 samples: (a) H-1; (b) H-2; (c) H-4; (d) H-10; (e) H-0.5; and (f) H-0.25 synthesized with different amount of solvent at 383 K

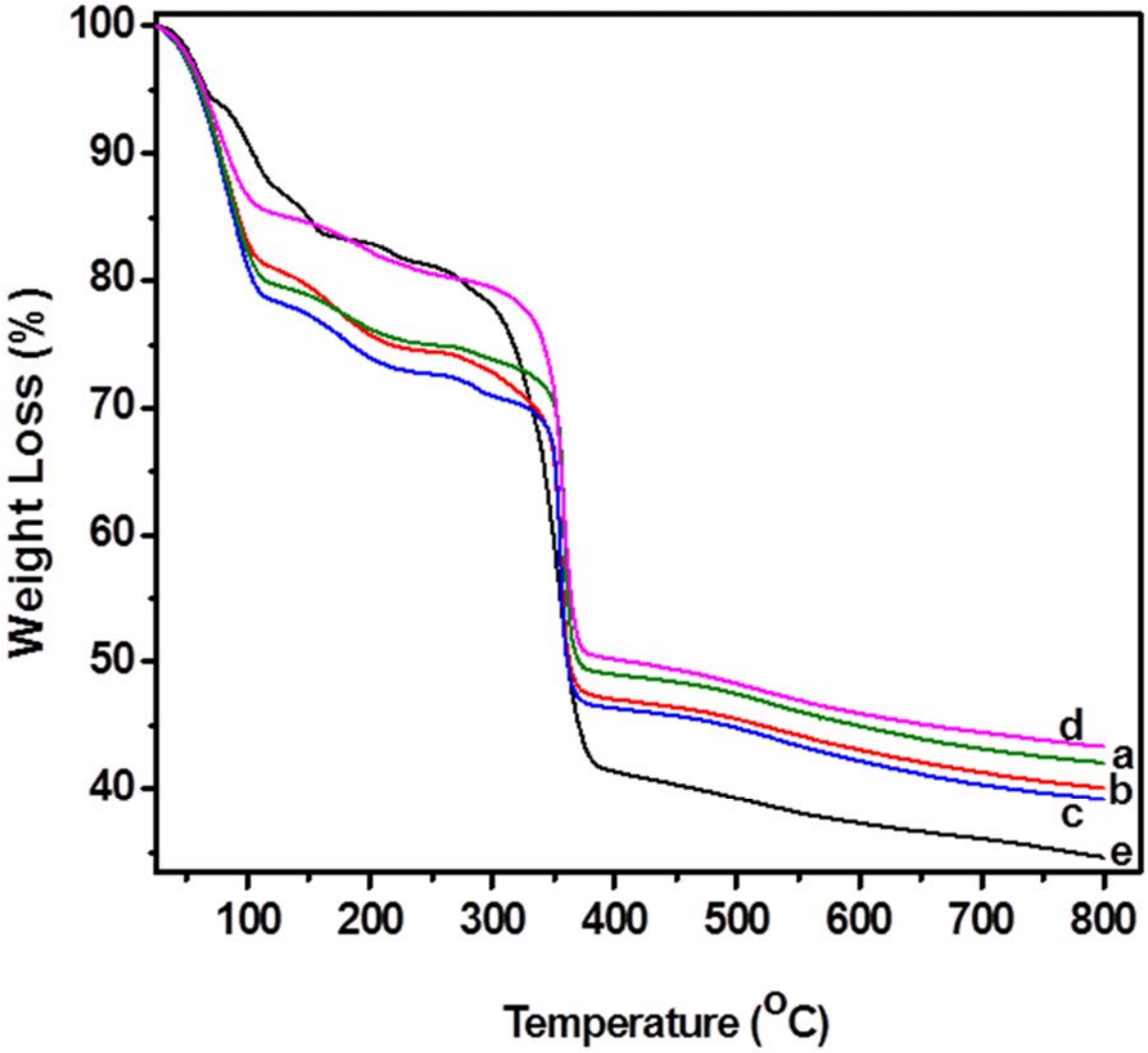

Figure 5. TG curves of as-made HKUST-1 samples in N_2: (a) H-1; (b) H-2; (c) H-4; (d) H-10; and (e) H-0.5

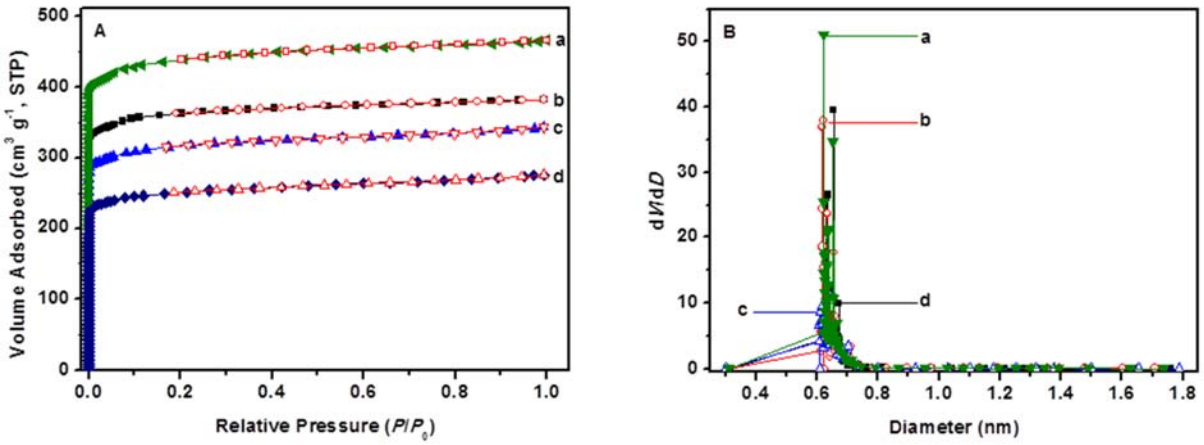

Figure 6. N_2 adsorption-desorption isotherms (A) and pore size distributions (B) of samples: (a) H-1; (b) H-2; (c) H-4; and (d) H-10

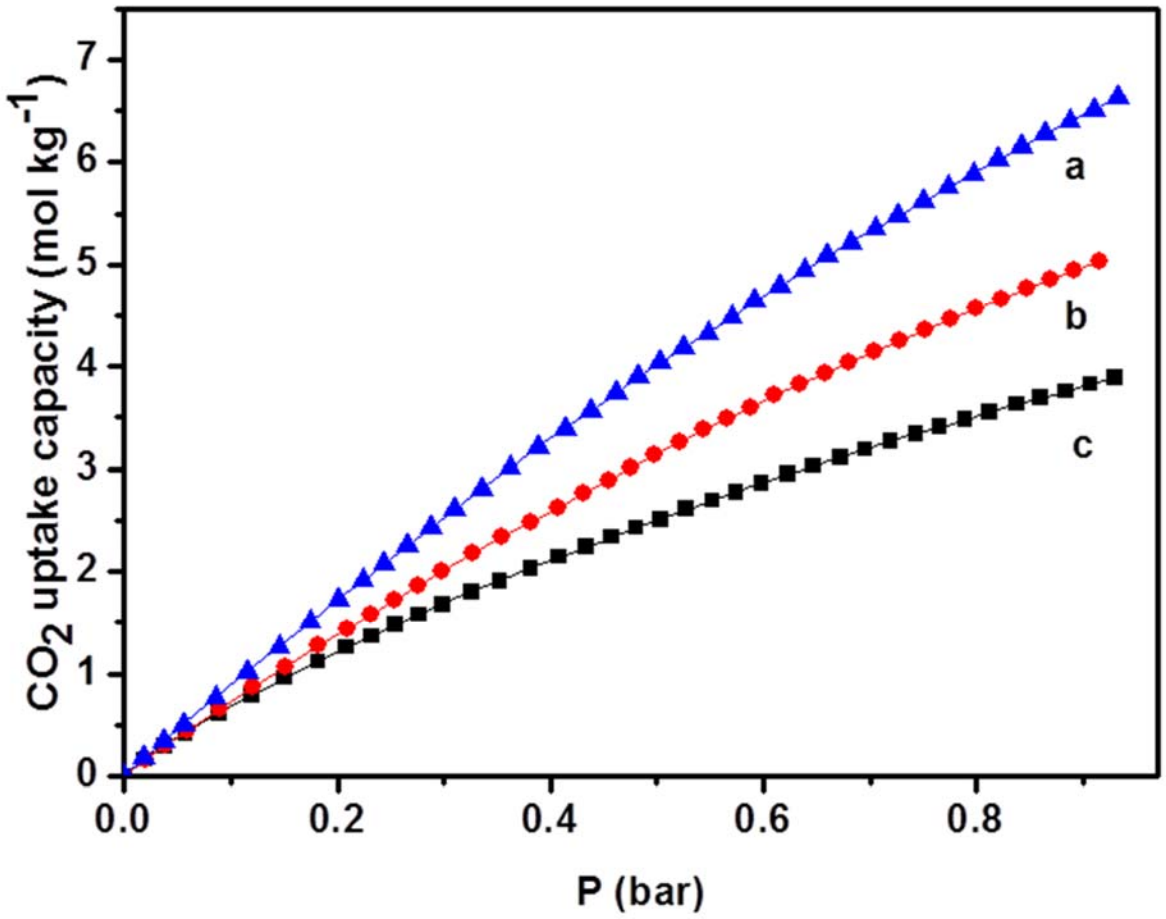

Figure 7. CO_2 gas adsorption isotherms at 295 K and pressure 0 – 1.0 bar on samples HKUST-1: (a) H-1; (b) H-2; and (c) H-4

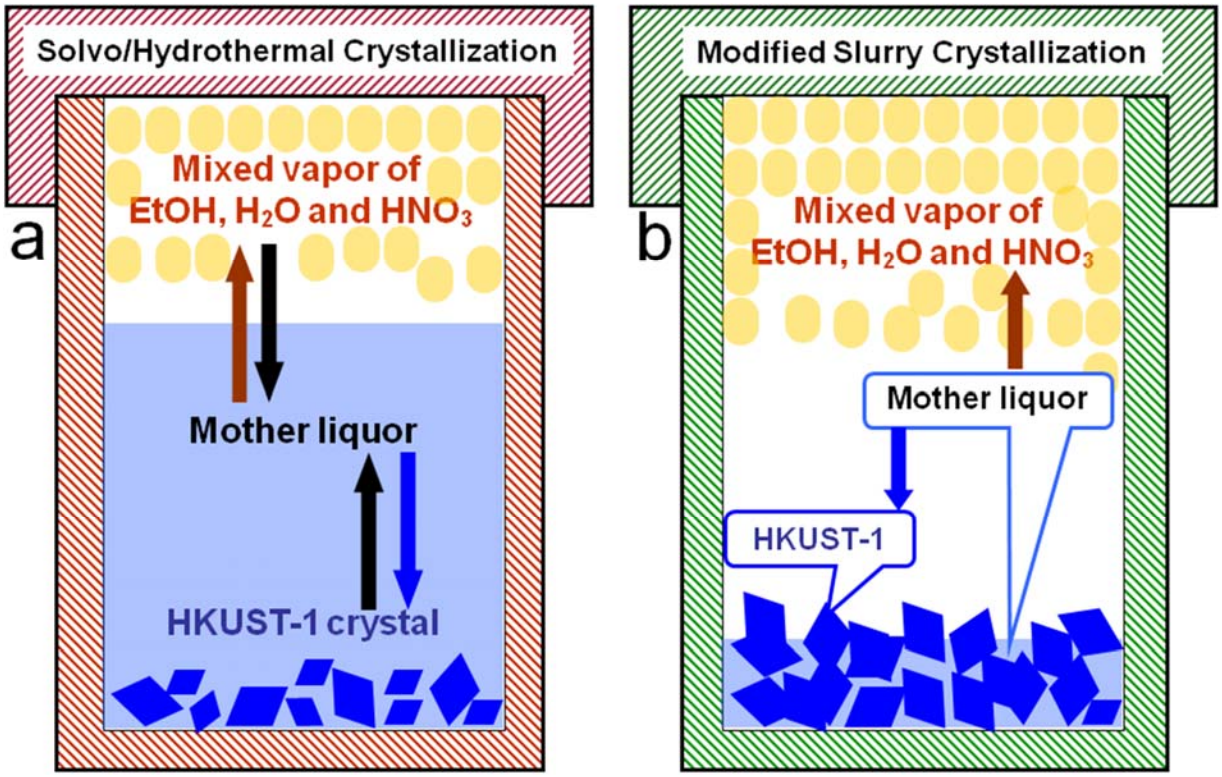

Figure 8. Schematic diagram of the crystallization methods for synthesizing HKUST-1: (a) solvo/hydrothermal process and (b) modified slurry crystallization process